This article has been accepted for publication in a future issue of this journal, but has not been fully edited. Content may change prior to final publication. Citation information: DOI 10.1109/TPEL.2015.2509962, IEEE Transactions on Power Electronics

Front End Monitoring of the Mutual Inductance and Load Resistance in a Series-Series Compensated Wireless Power Transfer System

Jian Yin, Deyan Lin, *Member, IEEE,* Thomas Parisini, *Fellow, IEEE,* and S. Y. (Ron) Hui, *Fellow, IEEE*

***Abstract*— In this paper a new method to estimate the mutual inductance and load resistance in a series-series compensated wireless power transfer system is presented. Reasonably accurate estimations can be obtained from measurements of the input voltage and current obtained at one operating frequency only. The proposal can be used to dynamically monitor both the coupling relationship between the transmitter and receiver coils and the load conditions without any direct measurement on the receiver side. It can also be used as a simple method to measure the mutual inductance of any pair of coupled coils. A novel impedance spectrum analysis method is further presented to show that series-series compensation has special characteristics in its input impedance spectrum. Experimental results with acceptable tolerance are included to verify the proposed method.**

***Index Terms*—Wireless power transfer, series-series compensation, impedance spectrum, mutual inductance estimation, load estimation.**

I. INTRODUCTION

Wireless power transfer (WPT) has found applications in consumer electronics, industrial manufacturing facilities and medical implants. Its potentials for charging electric vehicles have recently been actively explored. One common challenge faced in WPT applications is the information of the mutual coupling between the transmitter and receiver coils. For example, WPT systems with free-positioning feature are much more convenient than those with fixed-positioning one. However, free-positioning means that the receiver coil can be placed with some flexibility within the charging area. This implies that the relative position and hence the mutual inductance between the transmitter and receiver coils may not be the same each time. For dynamic WPT systems which have the load in motion, the mutual inductance is time-varying. The mutual coupling conditions between the transmitter and receiver coils are usually needed in order to achieve an optimal efficiency operation if the load is movable. To realize this feature, wireless feedback linking the transmitter and load sides [1]-[5] is usually needed, with the sensors installed on the load side.

Recently techniques employing only a single controller on the transmitter without any direct feedback from the output side have been presented. Such approach makes the WPT systems less sophisticated while keeping efficient system performance. References [6]-[8] make use of the simplified circuit model of a parallel-parallel (PP) compensated WPT system at the fixed resonant frequency to derive the load power by measuring the input voltage and current. This approach does not include the self-resistance of each coil and the model would fail if the input frequency deviates from the resonant frequency. In [9] and [10] an energy equilibrium function of a zero-voltage-switched (ZVS), secondary-series compensated WPT system is used to evaluate an estimation method for load variations. Several approximation steps are needed in this method and would affect the accuracy of the estimation results. In [11] a transient model of a series-series (SS) compensated WPT system is proposed to detect the initial load condition by injecting a series of high frequency signals before startup. However it does not track the load variations afterwards. In [12] a complete model describing the series-parallel (SP) compensated WPT system is proposed for performing online estimation of the mutual inductance, the value of the secondary-compensate capacitor and the electrical quantities on the secondary side by sampling the input voltage and current waveforms. Such method requires the measurements obtained from at least three different operating frequencies. In other words it is necessary to test the system under more than one input frequencies or adopt the harmonic components along with the fundamental one of the input voltage and current.

A recent paper [13] reports that in a WPT system with multiple coils, the load resistance could be uniquely determined by measuring the input voltage and current at one frequency only if the circuit parameters and coupling relations between every pair of coils are known. In this paper, research is extended to show that not only the load resistance but also the mutual inductance can be estimated simultaneously with the input voltage and current measurements at one operating frequency. This advantageous feature is applicable to SS compensation scheme. The proposed algorithm can be used as a simple experimental method to calculate the mutual inductance of any pair of coupled coils. A novel input impedance spectrum analysis method is adopted to demonstrate the special characteristics of the input impedance spectrum in the SS WPT system. Finally the experiment results are included to verify the proposal.

Manuscript received July 27, 2015; revised October 10, 2015; accepted December 2, 2015. This work was supported by the Hong Kong Research Grant Council under GRF Project 712913.

J. Yin is with Shenzhen Bronze Techologies, Shenzhen, China (e-mail: jyinee@hotmail.com).

D. Lin is with the Department of Electrical and Electronic Engineering, The University of Hong Kong, Hong Kong (e-mail: deyanlin@eee.hku.hk).

T. Parisini is with the Department of Electrical and Electronic Engineering, Imperial College London, London SW7 2AZ, U.K. He is also with the Department of Engineering and Architecture, University of Trieste, Trieste, 34127, Italy (e-mail: t.parisini@gmail.com).

S. Y. R. Hui is with the Department of Electrical and Electronic Engineering, The University of Hong Kong, Hong Kong. He is also with the Department of Electrical and Electronic Engineering, Imperial College London, London SW7 2AZ, U.K. (e-mail: ronhui@eee.hku.hk).

This article has been accepted for publication in a future issue of this journal, but has not been fully edited. Content may change prior to final publication. Citation information: DOI 10.1109/TPEL.2015.2509962, IEEE Transactions on Power Electronics

II. SERIES-SERIES COMPENSATION MODEL

A. Principles

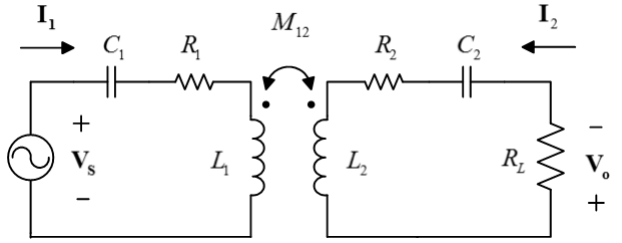

Fig. 1 Equivalent circuit of the two-coil SS compensated WPT system.

The equivalent circuit of the two-coil SS compensated WPT system is shown in Fig. 1, where R_1 and R_2 are the self-resistances of the primary and secondary coils, L_1 and L_2 are the self-inductances of the primary and secondary coils, C_1 and C_2 are the resonant capacitors which are connected in series with the primary and secondary coils respectively, M_{12} is the mutual inductance between the primary and secondary coils, R_L is the load resistance, $\mathbf{V_S}$ is the input voltage vector, $\mathbf{I_1}$ is the input current vector, and $\mathbf{V_o}$ and $\mathbf{I_2}$ are the vectors of the output voltage and current along the load R_L.

The system can be expressed in the matrix form as

$$\begin{bmatrix} \mathbf{V_S} \\ 0 \end{bmatrix} = \begin{bmatrix} Z_1 & j\omega M_{12} \\ j\omega M_{12} & Z_2 + R_L \end{bmatrix} \begin{bmatrix} \mathbf{I_1} \\ \mathbf{I_2} \end{bmatrix} \tag{1}$$

where $Z_1 = R_1 + j(\omega L_1 - \frac{1}{\omega C_1})$

$$Z_2 = R_2 + j(\omega L_2 - \frac{1}{\omega C_2})$$

ω is the angular frequency in the system.

Equation (1) consists of a nonlinear product term $R_L\mathbf{I_2}$, because both R_L and $\mathbf{I_2}$ are unknowns. It can be re-arranged by putting all the measureable terms ($\mathbf{V_S}$ and $\mathbf{I_1}$) to the left-hand side. Then, the original system equation can be transformed into the linear form,

$$\begin{bmatrix} \mathbf{V_S} - Z_1\mathbf{I_1} \\ -j\omega M_{12}\mathbf{I_1} \end{bmatrix} = \begin{bmatrix} j\omega M_{12} & 0 \\ Z_2 & 1 \end{bmatrix} \begin{bmatrix} \mathbf{I_2} \\ R_L\mathbf{I_2} \end{bmatrix} \tag{2}$$

Subsequently the unknown column vector on the right-hand side of (2) can be solved as follows:

$$\begin{bmatrix} \mathbf{I_2} \\ R_L\mathbf{I_2} \end{bmatrix} = \begin{bmatrix} j\omega M_{12} & 0 \\ Z_2 & 1 \end{bmatrix}^{-1} \times \begin{bmatrix} \mathbf{V_S} - Z_1\mathbf{I_1} \\ -j\omega M_{12}\mathbf{I_1} \end{bmatrix} = \begin{bmatrix} \dfrac{\mathbf{V_S} - Z_1\mathbf{I_1}}{j\omega M_{12}} \\ \dfrac{(\omega M_{12})^2\mathbf{I_1} + Z_1Z_2\mathbf{I_1} - Z_2\mathbf{V_S}}{j\omega M_{12}} \end{bmatrix} \tag{3}$$

So the load resistance can be expressed directly as

$$R_L = \frac{R_L\mathbf{I_2}}{\mathbf{I_2}} = \frac{(\omega M_{12})^2 + Z_1Z_2 - Z_2Z_{in}}{Z_{in} - Z_1} = \frac{(\omega M_{12})^2}{Z_{in} - Z_1} - Z_2 \tag{4}$$

where $Z_{in} = \dfrac{\mathbf{V_S}}{\mathbf{I_1}} = \dfrac{V_S}{I_1}\angle\varphi = |Z_{in}|\angle\varphi$ is the input impedance which can be expressed in the vector form.

It should be noted that the imaginary part of the right-hand side in (4) should be null because the load in the analysis is resistive. Therefore take the further deduction by equating its imaginary part to zero,

$$\mathbf{Im}\left(\frac{(\omega M_{12})^2}{Z_{in} - Z_1} - Z_2\right) = (\omega M_{12})^2\,\mathbf{Im}(Z_{in} - Z_1)^{-1} - (\omega L_2 - \frac{1}{\omega C_2}) = 0 \tag{5}$$

Then the mutual inductance can be derived as

$$M_{12} = \sqrt{\frac{\omega L_2 - \dfrac{1}{\omega C_2}}{\omega^2\,\mathbf{Im}(Z_{in} - Z_1)^{-1}}} \tag{6}$$

By substituting (6) into (4) the load resistance can be expressed in an equation independent of the mutual inductance,

$$R_L = \frac{\omega L_2 - \dfrac{1}{\omega C_2}}{(Z_{in} - Z_1)\,\mathbf{Im}(Z_{in} - Z_1)^{-1}} - Z_2 \tag{7}$$

Equations (6) and (7) show that if the self-parameters and the series resonant capacitor of each coil are given and assumed to be constant (i.e. R_1, R_2, L_1, L_2, C_1, C_2 are constant), and the amplitudes and phase shift of the input voltage and current can be measured at a specific operating frequency ω, then (i) the mutual inductance can be determined uniquely and (ii) the load resistance can be calculated. The other important electrical quantities on the secondary coil, such as the load voltage and current can also be derived from (3).

$$\mathbf{V_o} = R_L\mathbf{I_2} = \frac{(\omega M_{12})^2\mathbf{I_1} + Z_1Z_2\mathbf{I_1} - Z_2\mathbf{V_S}}{j\omega M_{12}} \tag{8}$$

$$\mathbf{I_2} = \frac{\mathbf{V_S} - Z_1\mathbf{I_1}}{j\omega M_{12}} \tag{9}$$

All the equations derived above are based on the measurement of the input voltage and current obtained at only one operating frequency. No additional frequency components are needed, and yet the instantaneous values of the mutual inductance and load can be estimated. Since it does not require the coupling information of the two coils, it implies that the relative positions of the transmitter and receiver (i.e. secondary) coils can change freely, thus making the proposed algorithm highly flexible. In addition there is no limitation on the selection of the frequency adopted except for the resonant frequency of the receiver coil, which will be explained later. Therefore the operating frequency could be adjustable to achieve better performance while the WPT system is in operation.

Although there are four kinds of fundamental compensation schemes [14] [15], only the SS compensation has the advantage of simply monitoring both the mutual inductance

This article has been accepted for publication in a future issue of this journal, but has not been fully edited. Content may change prior to final publication. Citation information: DOI 10.1109/TPEL.2015.2509962, IEEE Transactions on Power Electronics

and load resistance with front end measurement. The results in [12] have shown how complicated it is to achieve the same objective in an SP compensated WPT system. The SS compensation scheme takes this exclusive advantage in the system design of practical applications.

One typical application of the above concluded results is to find the mutual inductance of two coils in the space. Usually the mutual inductance can be calculated by means of approximated formulas or finite-element-method analysis [16]-[19]. However these methods are very complicated and not accurate enough in practical applications because the mutual inductance is related to many factors like the coil's sizes, shapes and relative positions. Therefore experimental method is desired. In this project, the mutual inductance can be directly calculated with (6) if series-compensated capacitors are used in the two coupled coils. If the two coils do not have their respective series-compensated capacitors, the original equation (6) will become:

$$M_{12} = \sqrt{\frac{\omega L_2}{\omega^2 \mathbf{Im}(Z_{in} - R_1 - j\omega L_1)^{-1}}} \qquad (10)$$

Thereby the mutual inductance between a pair of coils can be obtained by experimentally measuring the input voltage and current of any one coil.

B. Sensitivity Analysis

It can be observed that when the operating frequency is equal to the resonant frequency of the secondary coil,

$$\omega = \omega_2^* = \frac{1}{\sqrt{L_2 C_2}} \qquad (11)$$

The numerator term in (6) is 0. Therefore the term $\mathbf{Im}(Z_{in} - Z_1)^{-1}$ in the denominator must be 0 as well so as to make the expression reasonable. More specifically, the expression for $(\omega M_{12})^2$ becomes an indeterminate form $\frac{0}{0}$ when $\omega = \omega_2^* = \frac{1}{\sqrt{L_2 C_2}}$, i.e.

$$(\omega M_{12})^2\Big|_{\omega=\omega_2^*} = \left.\frac{\omega L_2 - \frac{1}{\omega C_2}}{\mathbf{Im}(Z_{in} - Z_1)^{-1}}\right|_{\omega=\omega_2^*} = \frac{0}{0} \qquad (12)$$

Generally the indeterminate form can be solved by the L'Hospital's Rule, i.e. taking the derivatives of both the numerator and denominator and making the division. However it does not work here because the term Z_{in} in the denominator comes from practical measurement. Z_{in} is not a constant because the input impedance is inherently related to the angular frequency. Z_{in} is also related to the two unknowns M_{12} and R_L. Therefore the partial derivative of Z_{in} with respect to the angular frequency ω cannot be written down in an explicit form while M_{12} and R_L are not given. The L'Hospital's Rule cannot be used to solve the indeterminate form in (12). Consequently (6) and (7) have no solutions at the resonant frequency of the receiver coil. Therefore, the method proposed here should avoid using ω_2^*. In practice, the operating frequency needs not be the exact value of the resonant frequency of the receiver circuit, especially when the coil has high quality factor. Using an operating frequency close to the ideal resonant one is usually acceptable without sacrificing the energy efficiency. Thus, the mutual inductance and load resistance can be calculated with (6) and (7) theoretically if the frequency is not the resonant frequency of the receiver.

However the existence of the unsolvable or singular frequency point affects the accuracy of the estimations. Fig. 2(a) is a general graph where the estimated results of the mutual inductance and load resistance over a wide frequency range from 520 kHz to 580 kHz are plotted with the secondary resonant frequency set at 552 kHz. It can be observed that within the interval from 548 kHz to 556 kHz (±4 kHz or ±0.7% of 552 kHz), the estimation results have tremendous errors which are not acceptable. Outside this small frequency range, the estimated results are sufficiently accurate. Fig. 2(b) shows an example of a lower secondary resonant frequency (about 252 kHz). The narrow range that is highly sensitive and inaccurate is ±2 kHz or ±0.8% of 252 kHz.

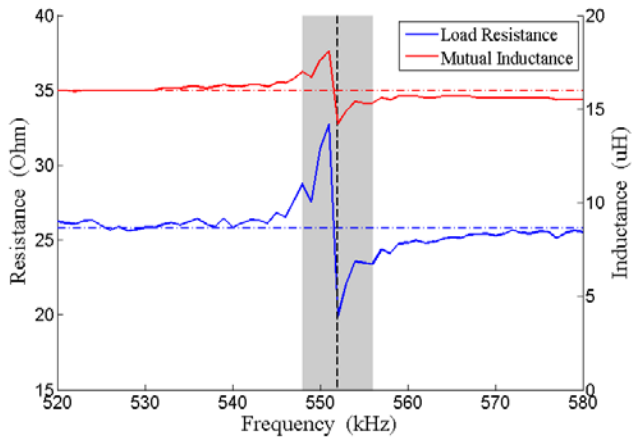

(a)

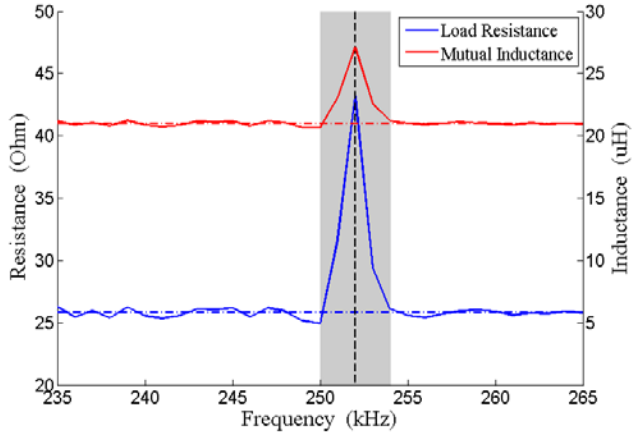

(b)

Fig. 2 Estimation results of the mutual inductance and load resistance. (a) Secondary resonant frequency 552 kHz. (b) Secondary resonant frequency 252 kHz.

III. INPUT IMPEDANCE ANALYSIS

According to the previous discussion, the mutual inductance

This article has been accepted for publication in a future issue of this journal, but has not been fully edited. Content may change prior to final publication. Citation information: DOI 10.1109/TPEL.2015.2509962, IEEE Transactions on Power Electronics

and load resistance can be uniquely determined based on the measurement of Z_{in} at one specific frequency except for the resonant frequency of the receiver coil (preferably outside the narrow range centered on the resonant frequency). It is necessary to analyze the frequency spectrum of the input impedance of a given WPT system. The impedance can be expressed as a vector on the complex plane where the real axis coordinate indicates the equivalent resistance of the impedance and the imaginary axis coordinate indicates its equivalent reactance. Alternatively the length of the vector is the amplitude of the impedance $|Z_{in}|$ and the angular displacement of the vector is the phase angle of the impedance $\angle\varphi$ on the polar-coordinate plane. By sweeping the frequency, a trajectory describing the variation of both the amplitude and the phase angle of the impedance with the frequency can be obtained, as shown in Fig. 3(a). However such a trajectory does not include the frequency information. Another axis perpendicular to the real-imaginary plane is needed to indicate the frequency of every impedance. Thus the impedance spectrum can be expressed in 3D space as shown in Fig. 3(b), where the red curve is the impedance spectrum and its projection on the bottom plane is identical to the blue curve in Fig. 3(a).

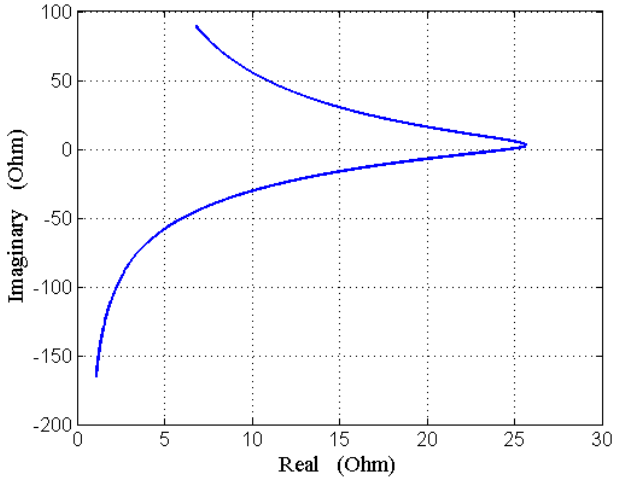

(a)

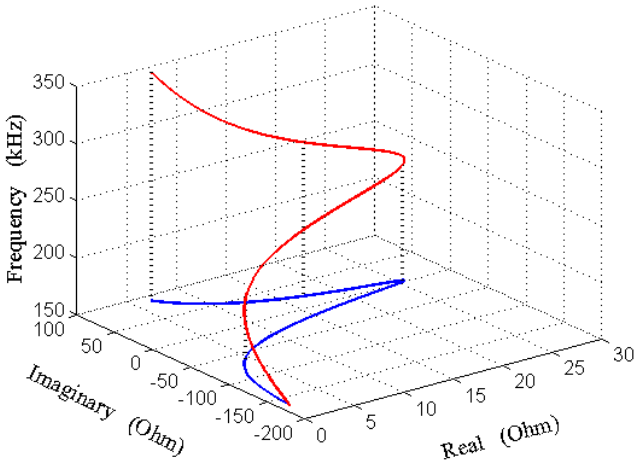

(b)

Fig. 3 Input impedance spectrum. (a) Impedance spectrum on a plane. (b) Impedance spectrum in a space.

Consider a fixed SS compensated WPT system whose circuit parameters are all constant while the mutual inductance and load resistance can be variable. If the mutual inductance is a known constant (M_{12} = 17 μH) and the load resistance is gradually increased, a series of input impedance spectral curves can be drawn as shown in Fig. 4(a). Since the mutual inductance is known, (6) is not needed and there is no problem with singularity issue at the resonant frequency. While the curves in Fig. 4(a) look as if they may tangle with one another, close examination indicates that they have no common points. Fig. 4(a) can be divided into two 2D graphs, namely the amplitude-frequency plot in Fig. 4(b) and the phase-frequency plot in Fig. 4(c). While the amplitude curves in Fig. 4(b) seem to have intersection points, their corresponding angles in Fig. 4(c) show that they are not the same. Fig. 5 illustrates another case where the load is kept constant (R_L=45 Ω) and the mutual inductance is varied. This graph shows more clearly that there is no common point among these curves.

For an SS compensated system, the trajectory of the input impedance is uniquely determined by its mutual inductance and load resistance according to the proposed method if only the measurements from the transmitter side are used and a frequency different from the resonant one is adopted. The impedance trajectory does not intersect with and is not tangential to the other trajectories except at the resonant frequency of the receiver coil. This is the reason why the mutual inductance and load resistance can be uniquely determined based on the sample of the input impedance at only one frequency.

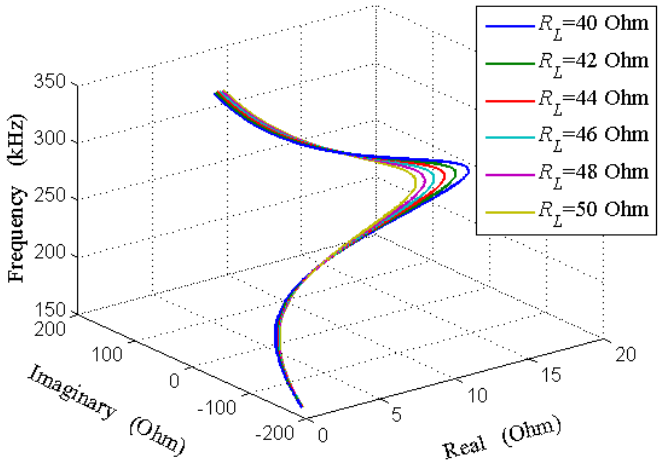

(a)

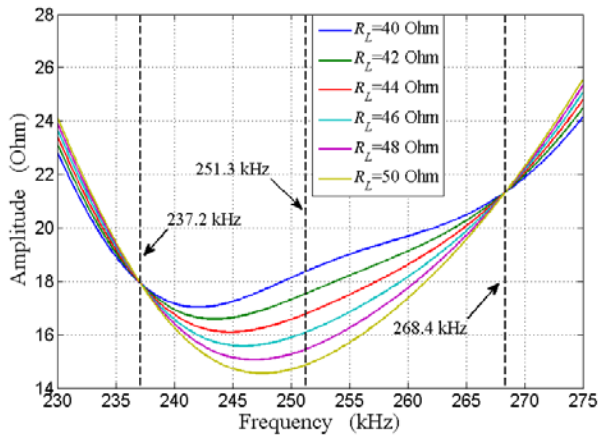

(b)

This article has been accepted for publication in a future issue of this journal, but has not been fully edited. Content may change prior to final publication. Citation information: DOI 10.1109/TPEL.2015.2509962, IEEE Transactions on Power Electronics

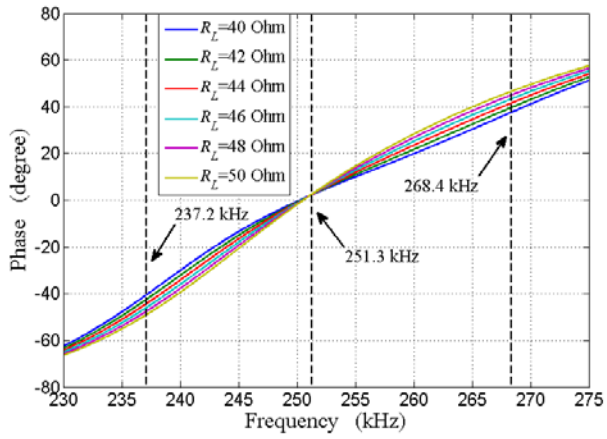

(c)

Fig. 4 Input impedance spectral characteristics for different load resistances. (a) 3D input impedance spectrum. (b) Amplitude-frequency spectrum. (c) Phase-frequency spectrum.

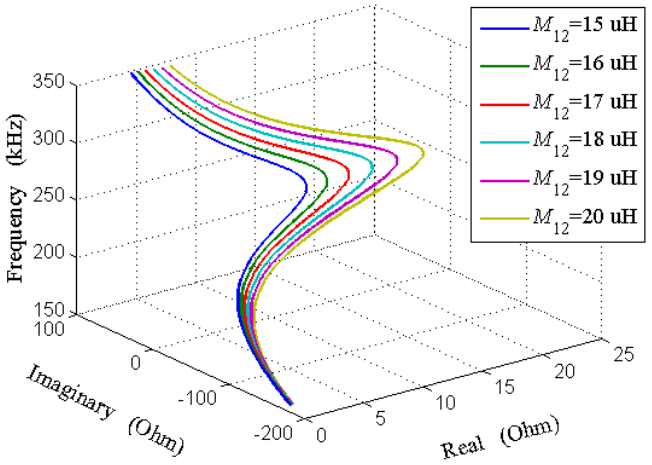

Fig. 5 Input impedance spectral characteristics for different mutual inductances.

Now consider the trajectory plots based on the proposed method in which (6) for M_{12} and (7) for R_L are used. In Fig. 6(a) a series of input impedance curves for an SS compensated WPT system are plotted for three values of mutual inductance. These curves meet at three points on the resonant frequency plane of 252 kHz. These intersections imply multiple solutions based on different M_{12} and R_L combinations. For example, when the same circuit parameters as listed in section IV are used, the resonant frequency of the receiver circuit is 251.79 kHz, which is the dark plane in Fig. 6(a). If the input impedance is 25.02∠2.54° Ω, there are infinite sets of likely M_{12} and R_L which lead to the same impedance value, such as M_{12}=14 μH, R_L=19.50 Ω; M_{12}=16 μH, R_L=25.66 Ω; M_{12}=18 μH, R_L=32.65 Ω, etc. One more example is that if the input impedance is 20.03∠3.18° Ω, the likely values of the mutual inductance and load resistance would be M_{12}=14 μH, R_L=24.70 Ω; M_{12}=16 μH, R_L=32.45 Ω; M_{12}=18 μH, R_L=41.23 Ω, and so on. The amplitude-frequency spectrum in Fig. 6(b) and phase-frequency spectrum in Fig. 6(c) further illustrate that at the resonant frequency of the receiver circuit the curves in Fig. 6(a) have three common points. Another important conclusion is that although the input impedances at the resonant frequency of the receiver are different based on various sets of M_{12} and R_L, the values of their imaginary parts are identical (which are 1.11 Ω in Fig. 6(a)). Actually the imaginary part of the input impedance is equal to the reactance of the transmitter circuit at the resonant frequency of the receiver, namely $\omega_2^* L_1 - \frac{1}{\omega_2^* C_1}$. Therefore all the intersection points constitute a straight line in parallel with the real axis, which is the black dashed line in Fig. 6(a), and its imaginary-axis projection is equal to the reactance of the transmitter circuit at the receiver-resonant frequency. For a fixed WPT system with various sets of M_{12} and R_L, all the input impedance spectral curves will converge along such a straight line. If the parameters of the resonant coils are changed, the position of the converging line will change. However it must meet three limitations: (i) it is parallel with the real axis; (ii) its vertical-axis projection is equal to the resonant frequency of the receiver ω_2^*; and (iii) its imaginary-axis projection is equal to the reactance of the transmitter circuit at ω_2^*. The special characteristics of the input impedance spectrum illustrate why the indeterminate form in (12) cannot be solved mathematically.

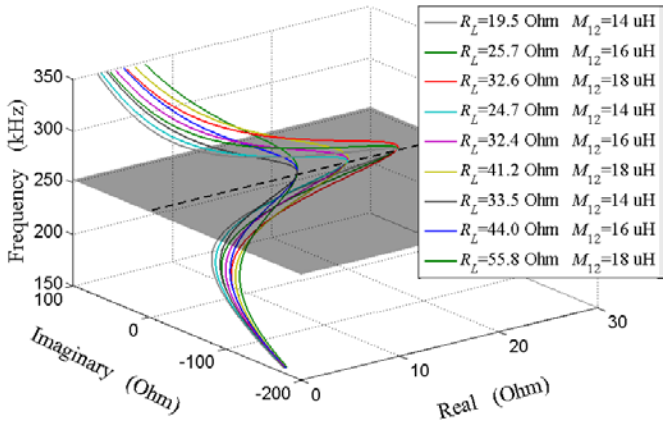

(a)

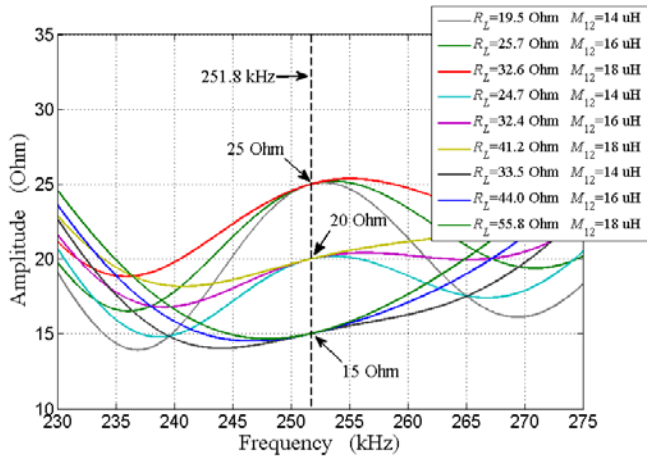

(b)

This article has been accepted for publication in a future issue of this journal, but has not been fully edited. Content may change prior to final publication. Citation information: DOI 10.1109/TPEL.2015.2509962, IEEE Transactions on Power Electronics

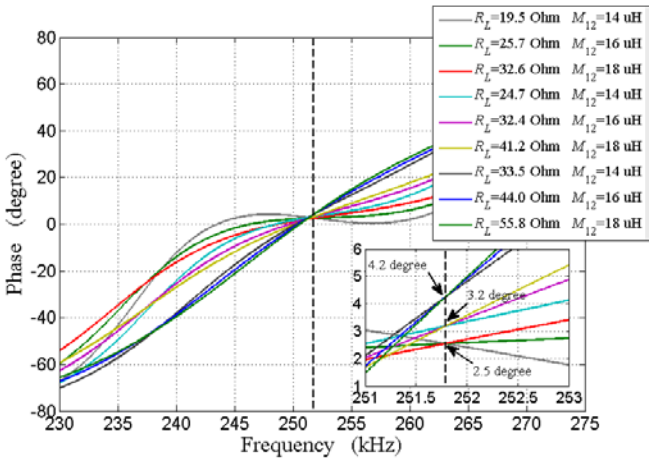

(c)

Fig. 6 Input impedance spectral curves meeting along the straight line on the resonant frequency plane. (a) 3D input impedance spectrum. (b) Amplitude-frequency spectrum. (c) Phase-frequency spectrum.

In contrast, the SP compensation shows different characteristics on the input impedance spectrum. Reference [12] reports that the samples of the input voltage and current at one frequency can lead to two likely sets of the mutual inductance and load resistance, both of which are mathematically correct to lead to the same input impedance. What is more, there is no limitation on the frequency. Thus two likely sets of solutions can be derived based on the sampled input impedance at any operating frequency. Graphically it indicates that the input impedance spectral curve would intersect with another curve at any operating frequency, not only at the receiver-resonant frequency as in the SS compensated system. In addition, there are infinite curves intersecting at the same input impedance point for the SS compensation. However for the SP compensation only two curves can join at one common point of the input impedance. Due to the special characteristics, the samples of the input voltage and current at two frequency components are necessary to uniquely determine the practical mutual inductance and load resistance in the SP system in [12].

IV. EXPERIMENTAL VERIFICATION

A two-coil WPT system has been constructed to verify the proposed parameter estimation method. The parameters of the primary coil are R_1=0.63 Ω, L_1=99.21 μH, and C_1=4.056 nF; the parameters of the secondary coil are R_2=0.63 Ω, L_2=99.44 μH, and C_2=4.018 nF. These parameters are measured by Agilent E5061B Network Analyzer. The coil diameter is 35 cm, and the number of turns is 11. Both the resonant capacitors are connected in series with their respective coils. The resonant frequency of the secondary resonator is around 251.79 kHz and the resonant frequency of the primary coil is 250.90 kHz. The input voltage, current and the phase angle of the WPT system required for the proposed method are captured by Tektronix DPO3034 Digital Oscilloscope (which has the de-skewing function for correcting measurement errors for high-frequency signals). These measurements are transferred to an external computer for the execution of the estimation algorithms for the calculation of M_{12}, R_L and the required input voltage V_1. The updated input voltage reference signal is fed to a function generator (Tektronix AFG3102) and then amplified linearly by AR 150A100B RF Amplifier. The output of the RF amplifier becomes the input voltage of the transmitter coil-resonator. The hardware setup for the experiment is shown in Fig. 7.

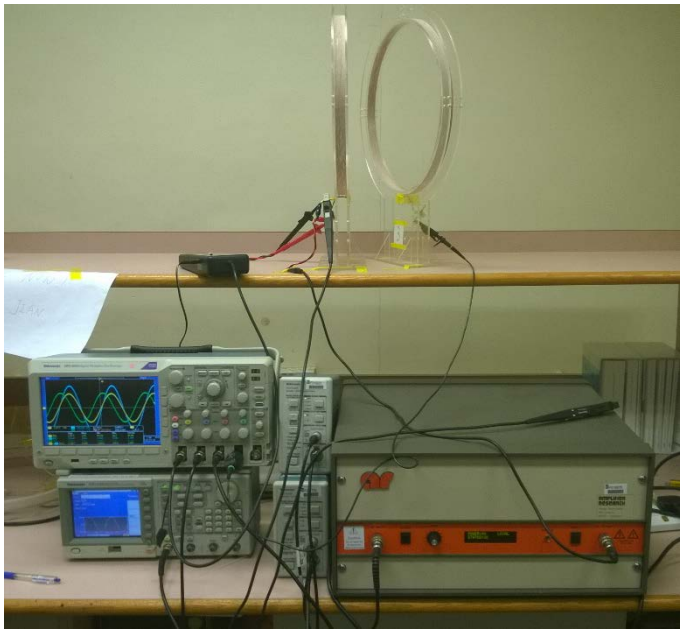

Fig. 7 Experiment setup.

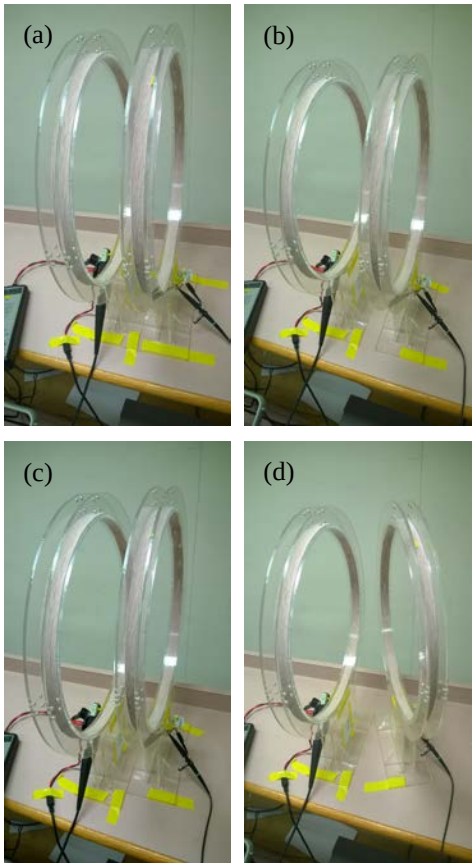

Fig. 8 Different coupling relations according to the different relative placements of the pair of coils. (a) Initial position. (b) Axial separation. (c) Lateral misalignment. (d) Angular misalignment.

A. Mutual Inductance and Load Estimation

In order to confirm the effectiveness of the estimation algorithm of the mutual inductance and load resistance, four arrangements of the transmitter and receiver coil-resonators with different relative positions shown in Fig. 8 have been used

This article has been accepted for publication in a future issue of this journal, but has not been fully edited. Content may change prior to final publication. Citation information: DOI 10.1109/TPEL.2015.2509962, IEEE Transactions on Power Electronics

for practical evaluation. For each case, the operating input frequency is scanned from 246 kHz to 258 kHz in discrete increment of 2 kHz. A load resistor of 25.8 Ω is used in these four cases. The estimation results are plotted in Fig. 9(a) to Fig. 9(d). As expected, the mutual inductance values in these four cases are different. The estimated values of M_{12} and R_L are accurate outside the narrow frequency range of 252 kHz ±2 kHz.

A second set of similar tests have been conducted with a load resistor of 17.4 Ω and four different relative positions. The measured and estimated values of M_{12} and R_L are summarized in TABLE I to TABLE IV. Again, the estimated values of M_{12} and R_L are accurate outside the narrow frequency range of 252 kHz ±2 kHz in TABLE I to TABLE IV.

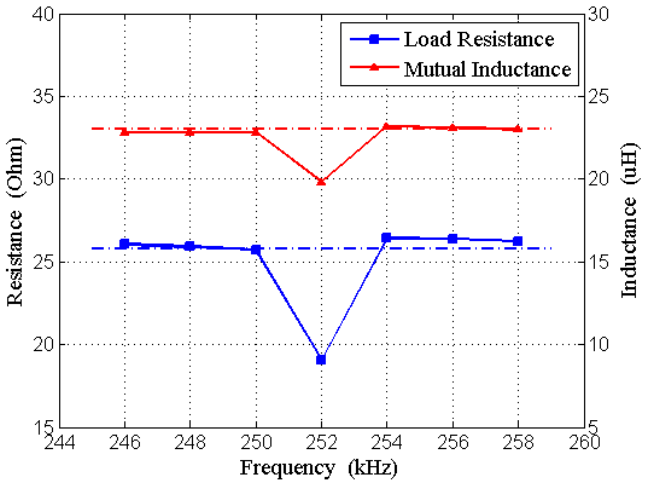

(a)

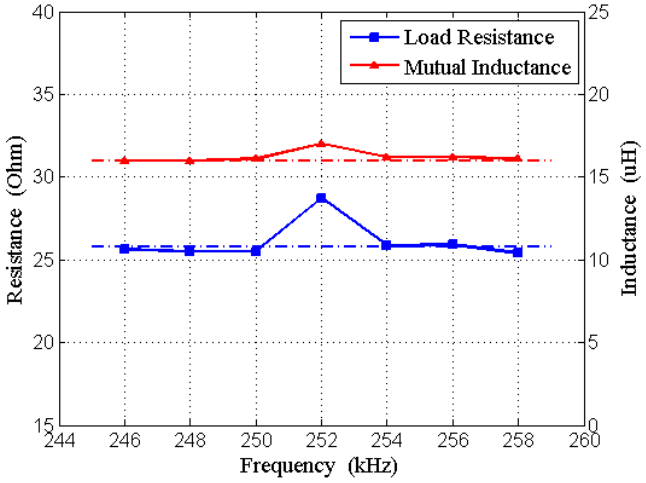

(b)

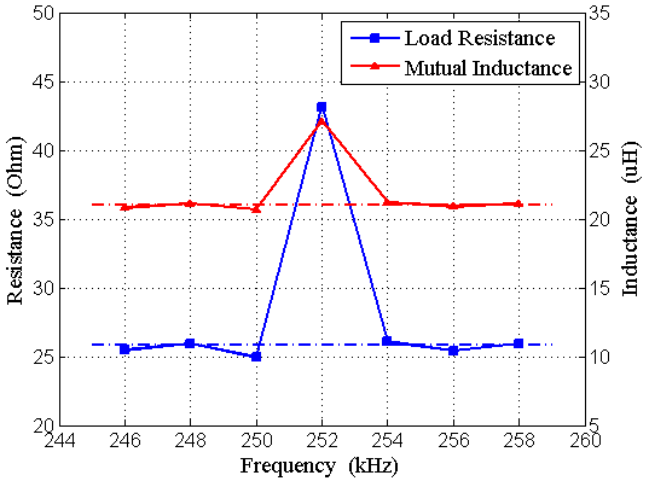

(c)

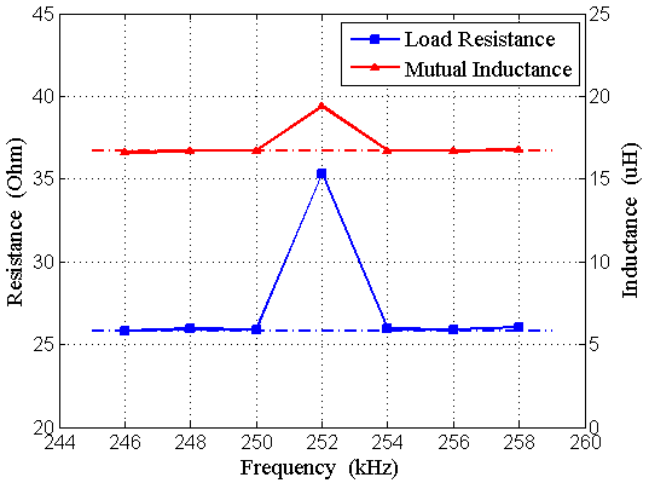

(d)

Fig. 9 Estimation results of the mutual inductance and load resistance. (a) Initial position (R_L=25.8 Ω, M_{12}=23.0 μH). (b) Axial separation (R_L=25.8 Ω, M_{12}=16.0 μH). (c) Lateral misalignment (R_L=25.8 Ω, M_{12}=21.0 μH). (d) Angular misalignment (R_L=25.8 Ω, M_{12}=16.7 μH).

TABLE I

INITIAL POSITION (R_L=17.4 Ω, M_{12}=23.0 μH)

	Operating Frequency (kHz)						
	246	248	250	252	254	256	258
$\lvert Z_{in}\rvert$ (Ω)	63.07	68.72	72.84	74.72	74.75	72.69	69.02
$\angle Z_{in}$ (deg)	16.6	11.7	6.3	0.5	-5.8	-11.2	-16.4
M_{12}^* (μH)	**23.0**	**23.1**	**22.8**	28.4	**23.0**	**23.1**	**23.0**
R_L^* (Ω)	**17.47**	**17.47**	**17.03**	26.59	**17.17**	**17.44**	**17.19**

TABLE II

AXIAL SEPERATION (R_L=17.4 Ω, M_{12}=13.7 μH)

This article has been accepted for publication in a future issue of this journal, but has not been fully edited. Content may change prior to final publication. Citation information: DOI 10.1109/TPEL.2015.2509962, IEEE Transactions on Power Electronics

	Operating Frequency (kHz)						
	246	248	250	252	254	256	258
$\lvert Z_{in}\rvert$ (Ω)	21.75	24.24	25.88	26.69	26.42	25.45	23.55
$\angle Z_{in}$ (deg)	5.8	5.8	4.3	2.1	-0.1	-1.7	-2.6
M_{12}^* (μH)	**13.7**	**13.8**	**13.8**	13.5	**13.7**	**13.8**	**13.6**
R_L^* (Ω)	**17.76**	**17.79**	**17.82**	16.81	**17.61**	**17.73**	**17.28**

TABLE III

LATERAL MISALIGNMENT (R_L=17.4 Ω, M_{12}=20.0 μH)

	Operating Frequency (kHz)						
	246	248	250	252	254	256	258
$\lvert Z_{in}\rvert$ (Ω)	51.41	56.42	59.75	61.48	61.03	59.09	56.00
$\angle Z_{in}$ (deg)	15.3	11.2	5.7	0.8	-4.7	-9.7	-14.4
M_{12}^* (μH)	**20.8**	**20.8**	**21.3**	27.6	**21.3**	**21.1**	**20.9**
R_L^* (Ω)	**17.53**	**17.26**	**18.07**	30.68	**18.10**	**17.87**	**17.51**

TABLE IV

ANGULAR MISALIGNMENT (R_L=17.4 Ω, M_{12}=17.7 μH)

	Operating Frequency (kHz)						
	246	248	250	252	254	256	258
$\lvert Z_{in}\rvert$ (Ω)	35.72	39.39	41.94	43.15	42.73	41.42	38.62
$\angle Z_{in}$ (deg)	12.2	9.3	5.3	1.5	-3.3	-7.3	-10.6
M_{12}^* (μH)	**17.5**	**17.5**	**17.7**	28.0	**17.6**	**17.6**	**17.4**
R_L^* (Ω)	**17.67**	**17.61**	**17.84**	45.53	**17.72**	**17.63**	**17.45**

B. Output Voltage Monitoring and Implication on Energy Efficiency

(i) Output Voltage Monitoring

This section addresses the issues of output voltage monitoring and the energy efficiency related to an operating frequency outside the narrow band centered on the resonator frequency of the receiver circuit. For the output voltage monitoring, tests have been set up to demonstrate the use of the proposed front end monitoring method of the WPT system without using any direct measurements on the receiver side. The setup involves the two coils being coaxially placed initially as shown in Fig. 8(a). The WPT system is operated at a constant frequency outside the narrow sensitive frequency range. Then the receiver coil is moved away from the transmitter coil in a step-by-step manner, with a displacement of 0.5 cm for each step. In each arrangement, the input voltage and current are measured in order to obtain the estimated values of the current mutual inductance and load resistance. Since all the self-parameters of the WPT system are known, the output voltage across the load can be calculated with (8) as $V_o = \dfrac{\left|(\omega M_{12})^2 + Z_1 Z_2 - Z_2 Z_{in}\right|}{\omega M_{12} I_1}$ for a given input voltage V_S. In order to achieve the desired output voltage V_o^*, the appropriate input voltage V_S^* should be $V_S^* = \dfrac{V_S V_o^*}{V_o}$. Consequently the estimated output voltage can be derived and used as a feedback variable in closed-loop control if desired.

In this set of experiments, the targeted output voltage across the load is set at 6 Vrms (for different positions of the receiver coil.) With the receiver coil being progressively placed away from the transmitter coil, the mutual inductance is expected to decrease. Initially a constant resistor of 25.8 Ω is used as the load. When the receiver coil is placed 4 cm away from the transmitter coil, the load resistor is changed to 17.4 Ω. The proposed method determines the required input voltage in each case to alter the input voltage in order to keep the estimated output voltage close to the desired value of 6 Vrms. The practical applied input voltage and the measured output voltage for each receiver position are plotted in Fig. 10. The practical operating frequency is 250 kHz (i.e. 2 kHz away from the resonant frequency of 252 kHz). It can be seen that the output voltage can be kept close to the reference value. The corresponding estimation results of the mutual inductance and load resistance are shown in Fig. 11.

(ii) Energy Efficiency

The energy efficiency from the transmitter to the receiver is related to the coupling coefficient and the load conditions. Usually it reaches a peak value at or near the resonant frequency of the secondary coil. Fig. 12(a) and Fig. 12(b) show the energy efficiency curves as a function of frequency for a range of M_{12} for R_L=25.8 Ω and R_L=17.4 Ω, respectively. It can be seen that the reduction of energy efficiency at a frequency slightly away (e.g. 1%) from the resonant frequency is very small.

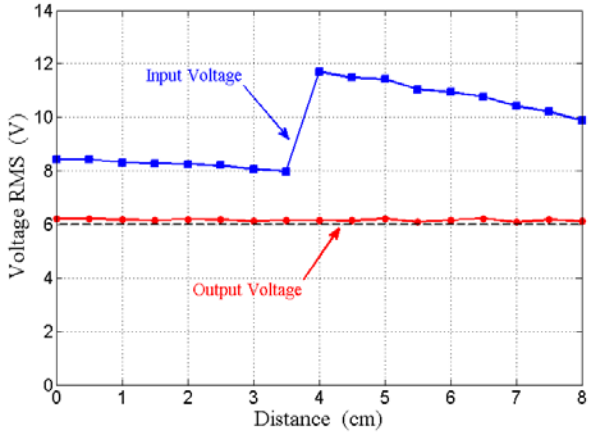

Fig. 10 Output voltage regulation.

This article has been accepted for publication in a future issue of this journal, but has not been fully edited. Content may change prior to final publication. Citation information: DOI 10.1109/TPEL.2015.2509962, IEEE Transactions on Power Electronics

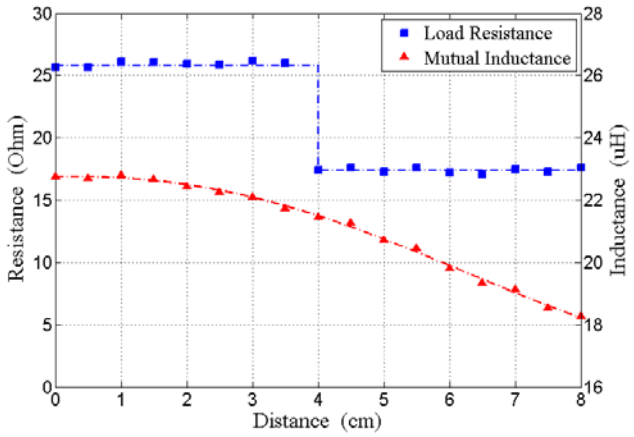

Fig. 11 Estimation results of the mutual inductance and load resistance.

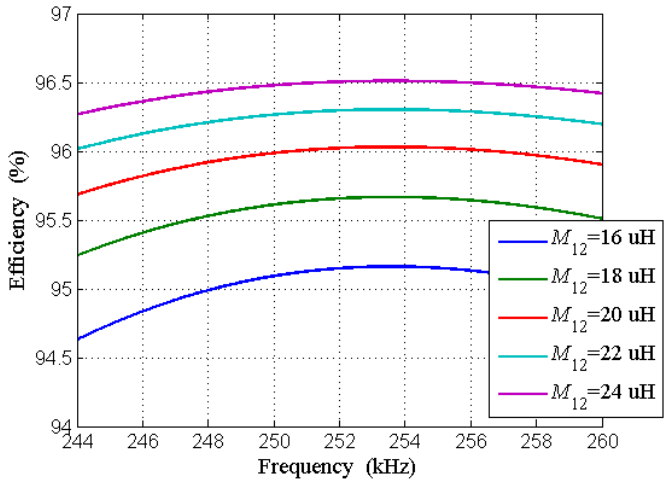

(a)

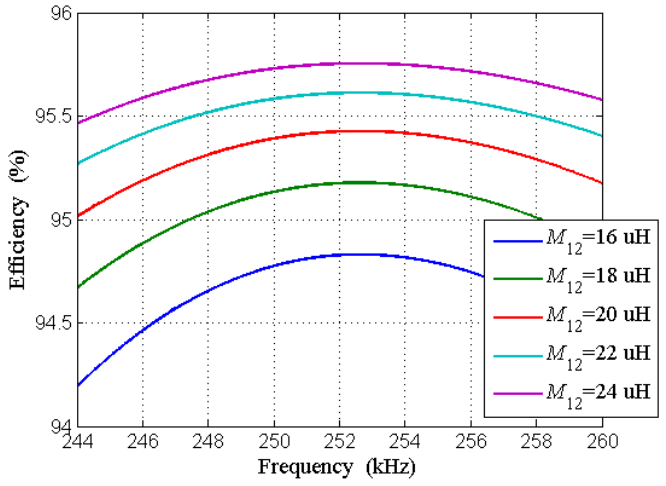

(b)

Fig. 12 Energy efficiency as a function of operating frequency under different coupling relations and load conditions. (a) R_L=25.8 Ω. (b) R_L=17.4 Ω.

C. Discussion on Sensitivity of Measurement and Parameter Errors

The estimations of M_{12} and R_L are sensitive to measurement errors and parameter tolerances. A detailed sensitivity analysis of a two-coil WPT system has been included in the Appendix. It is found that the estimation accuracy of the mutual inductance and load is more sensitive to the measured error in the phase angle than in the amplitude of the input impedance. For an operating frequency of a few hundred Kilo-Hertz, existing measurement technique (such as the de-skewing function in high-end digital storage oscilloscopes) is available for fairly accurate measurements, as demonstrated in the experimental results in this project. However, for a frequency of or higher than several Mega-Hertz, this may exist a practical limitation on accurate phase angle measurement. Nevertheless, it is a problem related to the measurement technique rather than the proposed algorithms. Regarding the circuit parameters, the estimation accuracy is sensitive to the errors of the self-inductance and resonant capacitance values. However, for both measurement and parameter errors, it is consistent that the sensitivity of the estimation accuracy is much reduced outside the narrow frequency band centered on the resonant frequency of the receiver circuit.

V. CONCLUSION

In this paper, a novel front end monitoring method of a SS compensated WPT system without the requirement of measurements on the receiver circuit is presented. This method involves new algorithms for calculating mutual inductance, load resistance and output voltage. For accurate estimation, it has been shown that the operating frequency for the estimation must not be the resonant frequency of the receiver circuit. In general, accurate estimation can be obtained by using a frequency outside a narrow frequency band centered on the resonant frequency, without sacrificing energy efficiency significantly. This narrow frequency band is typically ±1% of the resonant frequency. Since the proposed method can estimate both of the mutual inductance and the load, it is suitable for applications in which some degree of free-positioning is needed. An example is the wireless charging of electric vehicles. Experimental setups have been used for practical evaluation. The new proposed method has been favorably verified with experimental results.

APPENDIX

The equations can be expressed in terms of the measurements and parameters as follows:

$$M_{12}=\sqrt{\frac{(\omega L_2-\frac{1}{\omega C_2})[(|Z_{in}|\cos\varphi-R_1)^2+(|Z_{in}|\sin\varphi-\omega L_1+\frac{1}{\omega C_1})^2]}{-\omega^2(|Z_{in}|\sin\varphi-\omega L_1+\frac{1}{\omega C_1})}} \quad \text{(A1)}$$

$$R_L=-\frac{(\omega L_2-\frac{1}{\omega C_2})(|Z_{in}|\cos\varphi-R_1)}{|Z_{in}|\sin\varphi-\omega L_1+\frac{1}{\omega C_1}}-R_2 \quad \text{(A2)}$$

For the two-coil WPT system under investigation, the parameters of the primary coil are R_1=0.63 Ω, L_1=99.21 μH, and C_1=4.056 nF; the parameters of the secondary coil are R_2=0.63 Ω, L_2=99.44 μH, and C_2=4.018 nF. These parameters

This article has been accepted for publication in a future issue of this journal, but has not been fully edited. Content may change prior to final publication. Citation information: DOI 10.1109/TPEL.2015.2509962, IEEE Transactions on Power Electronics

$$\frac{\partial M_{12}}{\partial |Z_{in}|} = -\frac{M_{12}[-2(|Z_{in}|\cos\varphi - R_1)(|Z_{in}|\sin\varphi - \omega L_1 + \frac{1}{\omega C_1})\cos\varphi + (|Z_{in}|\cos\varphi - R_1)^2\sin\varphi - (|Z_{in}|\sin\varphi - \omega L_1 + \frac{1}{\omega C_1})^2\sin\varphi]}{2(|Z_{in}|\sin\varphi - \omega L_1 + \frac{1}{\omega C_1})[(|Z_{in}|\cos\varphi - R_1)^2 + (|Z_{in}|\sin\varphi - \omega L_1 + \frac{1}{\omega C_1})^2]} \quad \text{(A3)}$$

$$\frac{\partial M_{12}}{\partial \varphi} = -\frac{M_{12}|Z_{in}|[2(|Z_{in}|\cos\varphi - R_1)(|Z_{in}|\sin\varphi - \omega L_1 + \frac{1}{\omega C_1})\sin\varphi + (|Z_{in}|\cos\varphi - R_1)^2\cos\varphi - (|Z_{in}|\sin\varphi - \omega L_1 + \frac{1}{\omega C_1})^2\cos\varphi]}{2(|Z_{in}|\sin\varphi - \omega L_1 + \frac{1}{\omega C_1})[(|Z_{in}|\cos\varphi - R_1)^2 + (|Z_{in}|\sin\varphi - \omega L_1 + \frac{1}{\omega C_1})^2]} \quad \text{(A4)}$$

$$\frac{\partial R_L}{\partial |Z_{in}|} = -\frac{\omega^2 M_{12}^2[(\omega L_1 - \frac{1}{\omega C_1})\cos\varphi - R_1\sin\varphi]}{(|Z_{in}|\sin\varphi - \omega L_1 + \frac{1}{\omega C_1})[(|Z_{in}|\cos\varphi - R_1)^2 + (|Z_{in}|\sin\varphi - \omega L_1 + \frac{1}{\omega C_1})^2]} \quad \text{(A5)}$$

$$\frac{\partial R_L}{\partial \varphi} = -\frac{\omega^2 M_{12}^2|Z_{in}|[|Z_{in}| - (\omega L_1 - \frac{1}{\omega C_1})\sin\varphi - R_1\cos\varphi]}{(|Z_{in}|\sin\varphi - \omega L_1 + \frac{1}{\omega C_1})[(|Z_{in}|\cos\varphi - R_1)^2 + (|Z_{in}|\sin\varphi - \omega L_1 + \frac{1}{\omega C_1})^2]} \quad \text{(A6)}$$

are identical to what are used in the experiments in section IV. The mutual inductance is 18 μH, and the load resistance is 20 Ω.

A. Influence of the Measured Variables

In practical applications the input voltage and current are measured and used to derive the input impedance, i.e. $Z_{in} = \frac{\mathbf{V_S}}{\mathbf{I_1}} = \frac{V_S}{I_1}\angle\varphi = |Z_{in}|\angle\varphi$. Equivalently the measured variables can be regarded as two variables, namely the amplitude of the input impedance $|Z_{in}|$ and the phase angle of the input impedance φ. This simplification can effectively reduce the complexity of the analysis. By taking the partial derivatives of M_{12} and R_L with regard to $|Z_{in}|$ and φ respectively, the rates of change of M_{12} and R_L with respect to measurement errors can be evaluated in (A3) to (A6).

The rates of changes in (A3) to (A6) are plotted in Fig. A1 to Fig. A4. In Fig. A1 the absolute value of $\frac{\partial M_{12}}{\partial |Z_{in}|}$ outside the narrow band around the resonant frequency of 252 kHz is very small, less than 0.5 μH/Ohm. This means that as long as the measurement error in $|Z_{in}|$ is under 0.72 Ohm, the relative estimation error in M_{12} can achieve less than 2% in this study. In most WPT applications the coupling between two resonant coils is very loose, and therefore 2% estimation error is accurate enough. The results in Fig. A1 to Fig. A4 suggest that the accuracy of the estimation results are more sensitive to the measurement of φ than the amplitude of the input impedance.

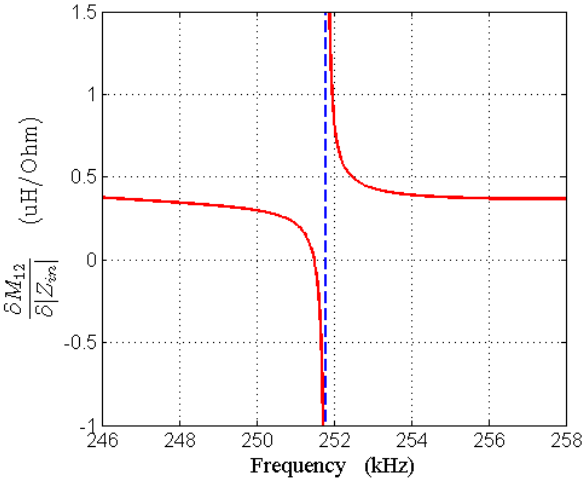

Fig. A1 Sensitivity of the estimated mutual inductance with respect to the amplitude of the input impedance.

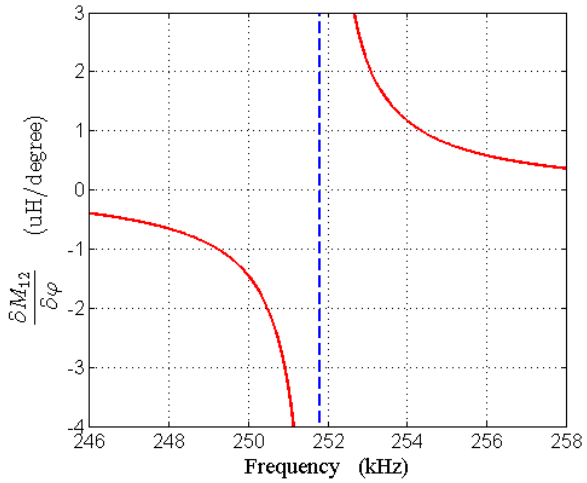

Fig. A2 Sensitivity of the estimated mutual inductance with respect to the phase angle of the input impedance.

This article has been accepted for publication in a future issue of this journal, but has not been fully edited. Content may change prior to final publication. Citation information: DOI 10.1109/TPEL.2015.2509962, IEEE Transactions on Power Electronics

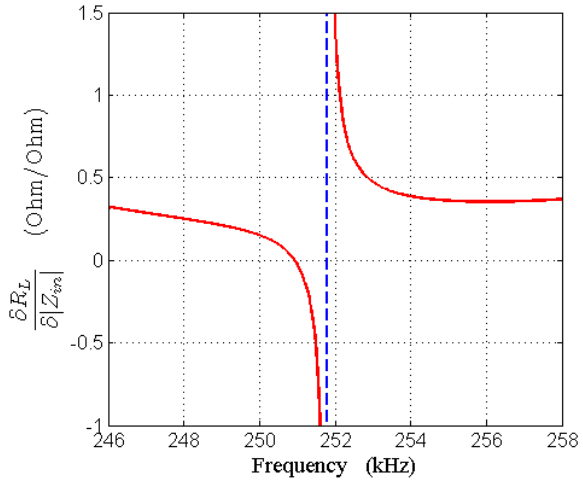

Fig. A3 Sensitivity of the estimated load resistance with respect to the amplitude of the input impedance.

In summary, the estimated M_{12} and R_L are very sensitive to the measurement errors in $|Z_{in}|$ and φ only within the small frequency range near the resonant frequency of the secondary coil. Outside the range the proposed algorithm can give stable and accurate estimation results even when some reasonable measurement errors exist in practice. The measurement of the phase angle φ has the more significant influence on the accuracy of the estimation than the input impedance amplitude $|Z_{in}|$.

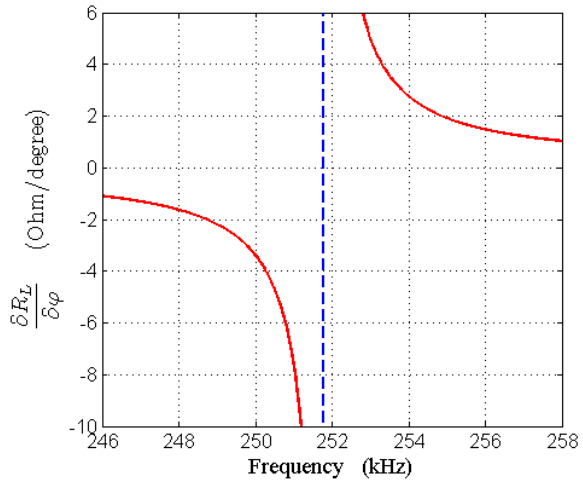

Fig. A4 Sensitivity of the estimated load resistance with respect to the phase angle of the input impedance.

B. Influence of the Parameter Variables

There are totally six parameter variables to consider (R_1, R_2, L_1, L_2, C_1, and C_2). They are regarded as constant parameters in the proposed algorithm. Let us examine the influence of R_1 and R_2 at first. Take the partial derivatives of M_{12} and R_L with respect to R_1 and R_2 individually.

$$\frac{\partial M_{12}}{\partial R_1} = -\frac{M_{12}(|Z_{in}|\cos\varphi - R_1)}{(|Z_{in}|\cos\varphi - R_1)^2 + (|Z_{in}|\sin\varphi - \omega L_1 + \frac{1}{\omega C_1})^2} \quad \text{(A7)}$$

$$\frac{\partial M_{12}}{\partial R_2} = 0 \quad \text{(A8)}$$

$$\frac{\partial R_L}{\partial R_1} = -\frac{(\omega M_{12})^2}{(|Z_{in}|\cos\varphi - R_1)^2 + (|Z_{in}|\sin\varphi - \omega L_1 + \frac{1}{\omega C_1})^2} \quad \text{(A9)}$$

$$\frac{\partial R_L}{\partial R_2} = -1 \quad \text{(A10)}$$

It is obvious that the mutual inductance is not related to R_2 from (A8). The rate of change of R_L with respect to R_2 is always -1 from (A10), meaning that 1 Ohm deviation of R_2 contributes to 1 Ohm deviation of R_L. The rates of change in (A7) and (A9) are plotted in Fig. A5 and Fig. A6 respectively. Although the curve of $\frac{\partial M_{12}}{\partial R_1}$ is monotonically increasing in Fig. A5, its absolute value is very small (i.e. less than 0.5 μH/Ohm from 250 to 254 kHz as shown in the enlarged graph). Hence during this frequency range 0.75 Ohm deviation of R_1 only leads to no more than 2% relative error in M_{12} in this study. Similarly, there is a peak in the $\frac{\partial R_L}{\partial R_1}$ curve around the resonant frequency of the secondary coil in Fig. A6, but its absolute value is less than 0.6 Ohm/Ohm within the small frequency range from 250 to 254 kHz. Therefore 1 Ohm deviation of R_1 only results in 0.6 Ohm deviation of R_L at most. In conclusion, R_1 and R_2 are not the dominant parameters that determine the accuracy of the estimated M_{12} and R_L. The proposed algorithm can provide reliable estimation results even when some reasonable errors in R_1 and R_2 exist in practice.

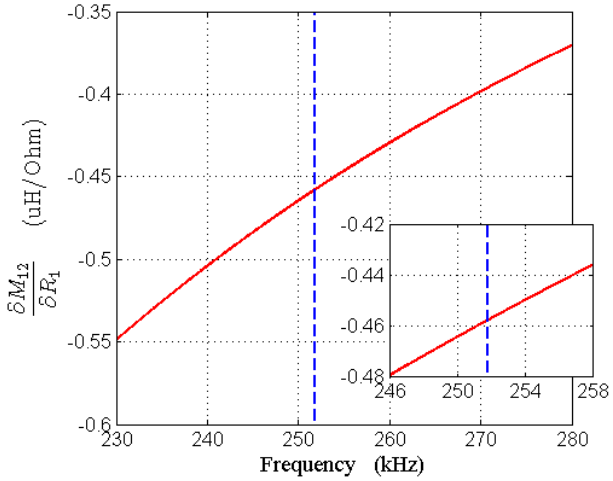

Fig. A5 Sensitivity of the estimated mutual inductance with respect to the resistance of the primary coil.

This article has been accepted for publication in a future issue of this journal, but has not been fully edited. Content may change prior to final publication. Citation information: DOI 10.1109/TPEL.2015.2509962, IEEE Transactions on Power Electronics

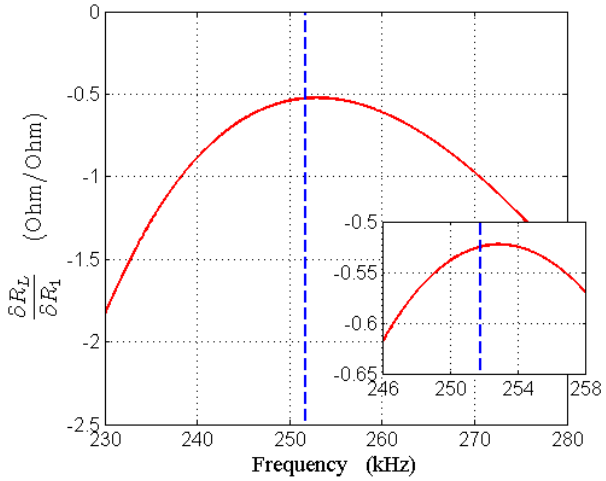

Fig. A6 Sensitivity of the estimated load resistance with respect to the resistance of the primary coil.

Now, the influence of L_1 and L_2 will be examined. Taking the partial derivatives of M_{12} and R_L with respect to L_1 and L_2 individually gives the following:

$$\frac{\partial M_{12}}{\partial L_1} = -\frac{\omega M_{12}[-(|Z_{in}|\cos\varphi - R_1)^2 + (|Z_{in}|\sin\varphi - \omega L_1 + \frac{1}{\omega C_1})^2]}{2(|Z_{in}|\sin\varphi - \omega L_1 + \frac{1}{\omega C_1})[(|Z_{in}|\cos\varphi - R_1)^2 + (|Z_{in}|\sin\varphi - \omega L_1 + \frac{1}{\omega C_1})^2]} \quad \text{(A11)}$$

$$\frac{\partial M_{12}}{\partial L_2} = -\frac{(|Z_{in}|\cos\varphi - R_1)^2 + (|Z_{in}|\sin\varphi - \omega L_1 + \frac{1}{\omega C_1})^2}{2\omega M_{12}(|Z_{in}|\sin\varphi - \omega L_1 + \frac{1}{\omega C_1})} \quad \text{(A12)}$$

$$\frac{\partial R_L}{\partial L_1} = \frac{\omega^3 M_{12}^2 (|Z_{in}|\cos\varphi - R_1)}{(|Z_{in}|\sin\varphi - \omega L_1 + \frac{1}{\omega C_1})[(|Z_{in}|\cos\varphi - R_1)^2 + (|Z_{in}|\sin\varphi - \omega L_1 + \frac{1}{\omega C_1})^2]} \quad \text{(A13)}$$

$$\frac{\partial R_L}{\partial L_2} = -\frac{\omega(|Z_{in}|\cos\varphi - R_1)}{|Z_{in}|\sin\varphi - \omega L_1 + \frac{1}{\omega C_1}} \quad \text{(A14)}$$

The results of (A11) to (A14) are plotted in Fig. A7 and Fig. A8. The sensitivity outside the narrow frequency band around the resonance frequency is limited. Such plots also provide information for the designers to choose the appropriate operating frequency in order to reduce the sensitivity. For example, if a frequency of 246 kHz is chosen, the sensitivity of M_{12} with L_1 and L_2 are limited to be less than ±2 μH/μH according to Fig. A7. Researchers interested in the proposed method should use their specific system parameters to conduct similar analysis and check if such sensitivity is acceptable.

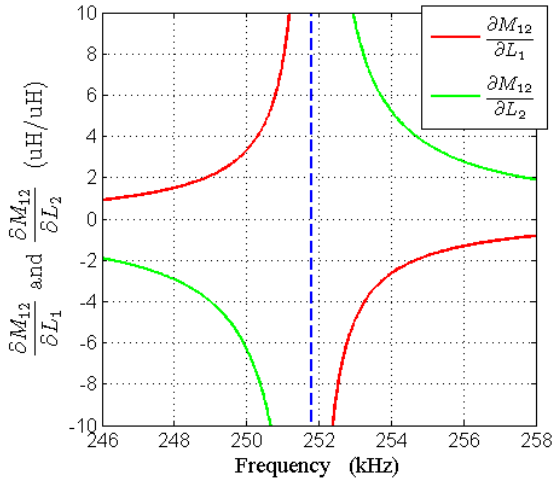

Fig. A7 Sensitivity of the estimated mutual inductance with respect to the inductances of the primary coil and the secondary coil.

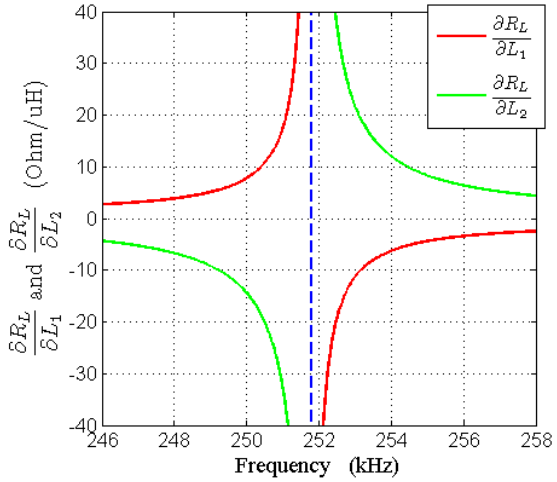

Fig. A8 Sensitivity of the estimated load resistance with respect to the inductances of the primary coil and the secondary coil.

Finally, the influences of C_1 and C_2 on the sensitivity are examined. Taking the partial derivatives of M_{12} and R_L with respect to C_1 and C_2 individually.

$$\frac{\partial M_{12}}{\partial C_1} = -\frac{M_{12}[-(|Z_{in}|\cos\varphi - R_1)^2 + (|Z_{in}|\sin\varphi - \omega L_1 + \frac{1}{\omega C_1})^2]}{2\omega C_1^2 (|Z_{in}|\sin\varphi - \omega L_1 + \frac{1}{\omega C_1})[(|Z_{in}|\cos\varphi - R_1)^2 + (|Z_{in}|\sin\varphi - \omega L_1 + \frac{1}{\omega C_1})^2]} \quad \text{(A15)}$$

$$\frac{\partial M_{12}}{\partial C_2} = -\frac{(|Z_{in}|\cos\varphi - R_1)^2 + (|Z_{in}|\sin\varphi - \omega L_1 + \frac{1}{\omega C_1})^2}{2M_{12}\omega^3 C_2^2 (|Z_{in}|\sin\varphi - \omega L_1 + \frac{1}{\omega C_1})} \quad \text{(A16)}$$

$$\frac{\partial R_L}{\partial C_1} = \frac{\omega M_{12}^2 (|Z_{in}|\cos\varphi - R_1)}{C_1^2 (|Z_{in}|\sin\varphi - \omega L_1 + \frac{1}{\omega C_1})[(|Z_{in}|\cos\varphi - R_1)^2 + (|Z_{in}|\sin\varphi - \omega L_1 + \frac{1}{\omega C_1})^2]} \quad \text{(A17)}$$

This article has been accepted for publication in a future issue of this journal, but has not been fully edited. Content may change prior to final publication. Citation information: DOI 10.1109/TPEL.2015.2509962, IEEE Transactions on Power Electronics

$$\frac{\partial R_L}{\partial C_2} = -\frac{|Z_{in}|\cos\varphi - R_1}{\omega C_2{}^2\left(|Z_{in}|\sin\varphi - \omega L_1 + \frac{1}{\omega C_1}\right)} \quad \text{(A18)}$$

The curves of $\frac{\partial M_{12}}{\partial C_1}$, $\frac{\partial M_{12}}{\partial C_2}$, $\frac{\partial R_L}{\partial C_1}$ and $\frac{\partial R_L}{\partial C_2}$ are plotted in Fig. A9 and Fig. A10. The same as the above analysis, the sensitivity outside the sensitive and narrow frequency band is limited.

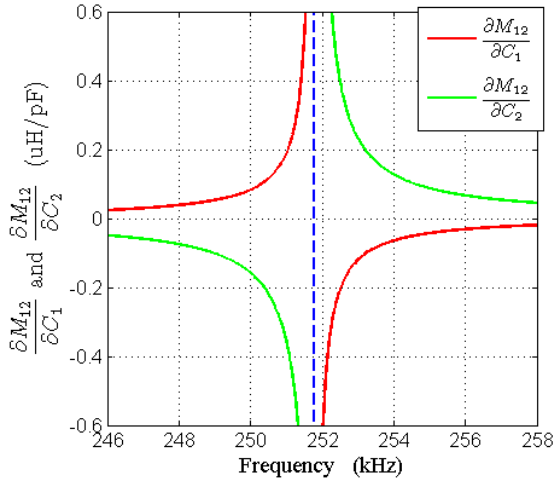

Fig. A9 Sensitivity of the estimated mutual inductance with respect to the capacitances of the primary coil and the secondary coil.

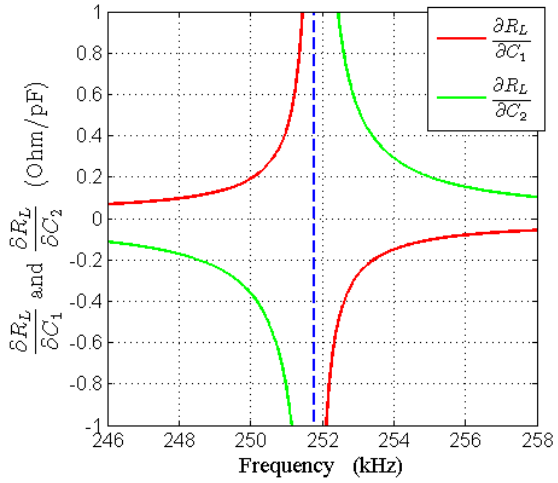

Fig. A10 Sensitivity of the estimated load resistance with respect to the capacitances of the primary coil and the secondary coil.

ACKNOWLEDGEMENT

The authors are grateful to the Hong Kong Research Grant Council for its support of the General Research Fund for Project 712913.

REFERENCES

[1] G. Wang, W. Liu, R. Bashirullah, M. Sivaprakasam, G. A. Kendir, Y. Ji, M. S. Humayun, and J. D. Weiland, "A closed loop transcutaneous power transfer system for implantable devices with enhanced stability," in *Proc. Int. Symp. Circuits Syst.*, May 2004, vol. 4, pp. IV: 17–20.

[2] P. Si, A. P. Hu, S. Malpas, and D. Budgett, "A frequency control method for regulating wireless power to implantable devices," *IEEE Trans. Biomed. Circuits Syst.*, vol. 2, no. 1, pp. 22–29, Mar. 2008.

[3] J. T. Boys, C.-Y. Huang, and G. A. Covic, "Single-phase unity power-factor inductive power transfer system," in *Proc. IEEE Power Electron. Spec. Conf. (PESC)*, Jun. 2008, pp. 3701–3706.

[4] H. L. Li, A. P. Hu, G. A. Covic, and C. Tang, "A new primary power regulation method for contactless power transfer," in *Proc. IEEE Int. Conf. Ind. Technol. (ICIT)*, Feb. 2009, pp. 1–5.

[5] N. Y. Kim, K. Y. Kim, J. Choi, and C.-W. Kim, "Adaptive frequency with power-level tracking system for efficient magnetic resonance wireless power transfer," *Electron. Lett.*, vol. 48, no. 8, pp. 452–454, Apr. 2012.

[6] U. K. Madawala, and D. J. Thrimawithana, "A single controller for inductive power transfer systems," in *Proc. IEEE IECON*, Nov. 2009, pp. 109–113.

[7] D. J. Thrimawithana, and U. K. Madawala, "A primary side controller for inductive power transfer systems," in *Proc. IEEE Int. Conf. Ind. Technol. (ICIT)*, Mar. 2010, pp. 661–666.

[8] U. K. Madawala, and D. J. Thrimawithana, "New technique for inductive power transfer using a single controller," *IET Power Electron.*, vol. 5, no. 2, pp. 248–256, Feb. 2012.

[9] X. Dai, Y. Sun, C. Tang, Z. Wang, Y. Su, and Y. Li, "Dynamic parameters identification method for inductively coupled power transfer system," in *Proc. IEEE Int. Conf. Sustainable Energy Technol. (ICSET)*, Dec. 2010, pp. 1–5.

[10] Z. Wang, X. Lv, Y. Sun, X. Dai, and Y. Li, "A simple approach for load identification in current-fed inductive power transfer system," in *Proc. IEEE Int. Conf. Power Syst. Technol. (POWERCON)*, Oct./Nov. 2012, pp. 1–5.

[11] Z. Wang, Y. Li, Y. Sun, C. Tang, and X. Lv, "Load detection model of voltage-fed inductive power transfer system," *IEEE Trans. Power Electron.*, vol. 28, no. 11, pp. 5233–5243, Nov. 2013.

[12] J. P. W. Chow, and H. S. H. Chung, "Use of primary-side information to perform online estimation of the secondary-side information and mutual inductance in wireless inductive link," in *Proc. IEEE Appl. Power Electron. Conf. Expo. (APEC)*, Mar. 2015, pp. 2648–2655.

[13] J. Yin, D, Lin, C. K. Lee, and S. Y. R. Hui, "A systematic approach for load monitoring and power control in wireless power transfer systems without any direct output measurement," *IEEE Trans. Power Electron.*, vol. 30, no. 3, pp. 1657–1667, Mar. 2015.

[14] C.-S. Wang, G. A. Covic, and O. H. Stielau, "Power transfer capability and bifurcation phenomena of loosely coupled inductive power transfer systems," *IEEE Trans. Ind. Electron.*, vol. 51, no. 1, pp. 148–157, Feb. 2004.

[15] C.-S. Wang, O. H. Stielau, and G. A. Covic, "Design considerations for a contactless electric vehicle battery charger," *IEEE Trans. Ind. Electron.*, vol. 52, no. 5, pp. 1308–1314, Oct. 2005.

[16] W. G. Hurley, and M. C. Duffy, "Calculation of self- and mutual inductances in planar sandwich inductors," *IEEE Trans. Magn.*, vol. 33, no. 3, pp. 2282–2290, May 1997.

[17] J. Acero, C. Carretero, I. Lope, R. Alonso, O. Lucia, and J. M. Burdio, "Analysis of the mutual inductance of planar-lumped inductive power transfer systems," *IEEE Trans. Ind. Electron.*, vol. 60, no. 1, pp. 410–420, Jan. 2013.

[18] J. Acero, C. Carretero, O. Lucia, R. Alonso, and J. M. Burdio, "Mutual impedance of small ring-type coils for multiwinding induction heating appliances," *IEEE Trans. Power Electron.*, vol. 28, no. 2, pp. 1025–1035, Feb. 2013.

[19] J. Acero, C. Carretero, I. Lope, R. Alonso, and J. M. Burdio, "Fea-based model of elliptic coils of rectangular cross section," *IEEE Trans. Magn.*, vol. 50, no. 7, pp. 1–7, Jul. 2014.

This article has been accepted for publication in a future issue of this journal, but has not been fully edited. Content may change prior to final publication. Citation information: DOI 10.1109/TPEL.2015.2509962, IEEE Transactions on Power Electronics

Jian Yin received the B.Eng. degree from Shandong University, Jinan, China, in 2007, and the Ph.D. degree from The University of Hong Kong, Hong Kong, in 2015.

He was an Electrical Engineer in the Grid Institute, Shandong Electric Power Engineering Consulting Institute, Jinan, China. Currently he is a Project Director in Shenzhen Bronze Technologies, Shenzhen, China. His research interests include sensorless motor drives and wireless power transfer technologies.

Deyan Lin (M'09) was born in China, in 1972. He received the B.Sc. and M.A.Sc. degrees from Huazhong University of Science and Technology, Wuhan, China, in 1995 and 2004, respectively, and the Ph.D. degree from the City University of Hong Kong, Kowloon, in 2012.

He is currently a Research Associate with the Department of Electrical and Electronic Engineering, The University of Hong Kong, Pokfulam. From 1995 to 1999, he was a Teaching Assistant in the Electrical Engineering Department at Jianghan University, Wuhan, where he became a Lecturer later. From 2008 to 2009, he was a Senior Research Assistant with the City University of Hong Kong. His current research interests include memristors, and modeling, control, simulation of gas-discharge lamps, and wireless power transfer.

Thomas Parisini (S'87–M'88–SM'99–F'11) received the Ph.D. degree in electronic engineering and computer science from the University of Genoa, Genova, Italy, in 1993.

He was with Politecnico di Milano, and since 2010 he holds the Chair of Industrial Control at Imperial College London. Since 2001, he has been the Danieli Endowed Chair of Automation Engineering with University of Trieste. In 2009-2012 he was the Deputy Rector of the University of Trieste. He authored or co-authored more than 250 research papers in archival journals, book chapters, and international conference proceedings. He is currently leading consultancy projects with some major process control companies (Danieli, Duferco, Electrolux, among others). His current research interests include neural-network approximations for optimal control problems, fault diagnosis for nonlinear and distributed systems, nonlinear model predictive control systems and nonlinear estimation.

Prof. Parisini is a co-recipient of the IFAC Best Application Paper Prize of the *Journal of Process Control*, Elsevier, for the three-year period 2011-2013 and of the 2004 Outstanding Paper Award of the IEEE Trans. on Neural Networks. He is also a recipient of the 2007 IEEE Distinguished Member Award. He is involved as Project Leader in several projects funded by the European Union, by the Italian Ministry for Research. In 2012 he was awarded a prestigious ABB Research Grant dealing with energy-autonomous sensor networks for self-monitoring industrial environments. He is the Editor-in-Chief of the IEEE Trans. on Control Systems Technology. He is also the Chair of the IFAC Technical Committee on Fault Detection, Supervision, and Safety of Technical Processes–SAFEPROCESS. He was a Distinguished Lecturer and an elected member of the Board of Governors of the IEEE Control Systems Society. Among other activities, he was the Program Chair of the 2008 IEEE Conference on Decision and Control and the General Co-Chair of the 2013 IEEE Conference on Decision and Control.

S. Y. (Ron) Hui (M'87–SM'94–F'03) received the B.Sc. (Eng. Hons.) degree from the University of Birmingham, Birmingham, U.K., in 1984, and the D.I.C. and Ph.D. degree from the Imperial College London, London, U.K., in 1987.

He currently holds the Philip Wong Wilson Wong Chair Professorship at the University of Hong Kong and a Chair Professorship at Imperial College London. He has authored or coauthored more than 300 technical papers, including more than 200 refereed journal publications. Over 55 of his patents have been adopted by industry.

Dr. Hui is an Associate Editor of the IEEE TRANSACTIONS ON POWER ELECTRONICS and IEEE TRANSACTIONS ON INDUSTRIAL ELECTRONICS, and an Editor of the IEEE JOURNAL OF EMERGING AND SELECTED TOPICS IN POWER ELECTRONICS. He was appointed twice as an IEEE Distinguished Lecturer by the IEEE Power Electronics Society in 2004 and 2006. He won the IEEE Best Paper Award from the IEEE IAS in 2002 and two IEEE Power Electronics Transactions Prize Paper Awards in 2009 and 2010. His inventions on wireless charging platform technology underpin key dimensions of Qi, the world's first wireless power standard, with freedom of positioning and localized charging features for wireless charging of consumer electronics. In November 2010, he received the IEEE Rudolf Chope R&D Award from the IEEE Industrial Electronics Society and the IET Achievement Medal (The Crompton Medal). He is a Fellow of the Australian Academy of Technological Sciences and Engineering and is the recipient of the 2015 IEEE William E. Newell Power Electronics Award.